Kinetics of Ligand Binding to the Type 1 Fc_ϵ Receptor on Mast Cells†

Enrique Ortega,‡ Reinhard Schweitzer-Stenner,§ and Israel Pecht*,‡

Department of Chemical Immunology, The Weizmann Institute of Science, Rehovot 76100, Israel, and Department of Physics, University of Bremen, 2800 Bremen 33, Federal Republic of Germany

Received September 6, 1990; Revised Manuscript Received December 5, 1990

ABSTRACT: Rates of association and dissociation of several specific monovalent ligands to and from the type I Fc_ϵ receptor ($Fc_\epsilon RI$) were measured on live mucosal type mast cells of the rat line RBL-2H3. The ligands employed were a monoclonal murine IgE and Fab fragments prepared from three different, $Fc_\epsilon RI$-specific monoclonal IgG class antibodies. These monoclonals (designated H10, J17, and F4) were shown previously to trigger mediator secretion by RBL-2H3 mast cells upon binding to and dimerization of the $Fc_\epsilon RI$. Analysis of the kinetics shows that the minimal mechanism to which all data can be fitted involves two consecutive steps: namely, ligand binding to a low-affinity state of the receptor, followed by a conformational transition into a second, higher affinity state h of the receptor–ligand complex. These results resolve the recently noted discrepancy between the affinity of IgE binding to the $Fc_\epsilon RI$ as determined by means of binding equilibrium measurements [Ortega et al. (1988) *EMBO J. 7*, 4101] and the respective parameter derived from the ratio of the rate constant of rat IgE dissociation and the initial rate of rat IgE association [Wank et al. (1983) *Biochemistry 22*, 954]. The probability of undergoing the conformational transition differs for the four different $Fc_\epsilon RI$–ligand complexes: while binding of Fab-H10 and IgE favors the h state, binding of Fab-J17 and Fab-F4 preferentially maintains the low-affinity l state (at 25 °C). The temperature dependence of the ligand interaction kinetics with the $Fc_\epsilon RI$ shows that the activation barrier for ligand association is determined by positive enthalpic and entropic contributions. The activation barrier of the l → h transition, however, has negative enthalpic contributions counteracted by a decrease in activation entropy. The h → l transition encounters a barrier that is predominantly entropic and similar for all ligands employed, thus suggesting that the $Fc_\epsilon RI$ undergoes a similar conformational transition upon binding any of the ligands.

It is increasingly appreciated that an in-depth understanding of the interactions between a cell surface receptor and its respective ligand requires that the kinetics of these processes have been studied. One of the cell receptor systems that has received considerable attention in this respect is the type I receptor for Fc_ϵ domains ($Fc_\epsilon RI$)[1] present on mast cells and basophils (Froese, 1984; Metzger et al., 1987). This receptor consists of four polypeptide chains: one α, and β, and two identical γ chains. The amino acid sequences of each of these have been recently deduced from cDNA sequences. The α subunit, earlier identified as directly binding the Fc_ϵ domains, most probably does so by its two Ig-like domains residing on the cell surface (Kinet et al., 1987). A single IgE molecule is bound per $Fc_\epsilon RI$ unit, apparently in an asymmetric and bent conformation (Holowka et al., 1985; Helm et al., 1988; Zheng et al., 1990).

The time course of IgE association with and dissociation from the $Fc_\epsilon RI$ has been investigated both because this interaction constitutes the initial step in the cascade of mast cell stimulation and since it represents an interesting model system, where a quantitative examination of monovalent ligand–receptor interactions can be made. Earlier studies of the $Fc_\epsilon RI$–IgE reaction mechanism led to the conclusion that it can be described by a single-step bimolecular binding and unimolecular dissociation process (Kulczycky & Metzger, 1974; Wank et al., 1983; Froese, 1984).

Recently, we have raised and characterized several monoclonal antibodies (mAbs) specific for the α subunit of the $Fc_\epsilon RI$ (Ortega et al., 1988). These mAbs were shown to be effective secretagogues of mast cells. Furthermore, being homogeneous divalent ligands, they enable a quantitative correlation between the stimulus produced by receptor–ligand interactions and the cellular response. We have indeed shown that these IgG class mAbs cross-link the $Fc_\epsilon RI$ on mucosal mast cells of the RBL-2H3 line to produce dimers only and that these were sufficient for inducing the secretory response. Moreover, quantitative analysis of receptor dimerization clearly suggested that the cellular response is determined not only by the number of $Fc_\epsilon RI$ dimers produced by each different mAb, but even more so by their intrinsic structural and dynamic properties (Ortega et al., 1988). Our experiments suggest that the secretion-inducing capacity of the examined mAbs could be primarily determined by the orientational constraints they impose on the dimerized $Fc_\epsilon RI$s and not by the lifetimes of the dimers (Ortega et al., 1988; Ortega, 1990).

In the present study we have analyzed in detail the kinetics of interaction between the $Fc_\epsilon RI$ on living RBL-2H3 cells and monovalent Fab fragments derived from three different $Fc_\epsilon RI$-specific mAbs (Ortega et al., 1988) and compared them with those of a monoclonal murine IgE. These experiments were carried out over a range of temperatures in order to determine the activation barriers characterizing these interactions.

† Financial support for the studies reported in this paper was generously provided by grants from The Fritz Thyssen Foundation, FRG, and the Council for Tobacco Research, U.S.A. (2799). During part of these studies, E.O. was the recipient of a scholarship from the Consejo Nacional de Ciencia y Tecnologia, Mexico (27696). R.S.-S. acknowledges the receipt of a short-term fellowship from the Minerva Foundation, FRG.

‡ The Weizmann Institute of Science.

§ University of Bremen.

[1] Abbreviations: RBL-2H3, rat basophilic leukemia cells, subline 2H3; SSM, single-state model; TSM, two-state model; FCS, fetal calf serum; mAb, monoclonal antibody; $Fc_\epsilon RI$, type I receptor for Fc_ϵ domains; AC, association rate curve; DCD, dissociation rate curve observed after sample dilution; DCDI, dissociation rate curve observed after sample dilution with excess unlabeled IgE.

0006-2960/91/0430-3473$02.50/0

THEORY

Here we present the theoretical framework employed in the analysis of the rates of association and dissociation of radioactively labeled monovalent ligands (Fab-J17, Fab-F4, Fab-H10, and IgE) to and from the $Fc_\epsilon RI$. First, the interaction kinetics of these ligands were analyzed in terms of the simplest mechanism, i.e., a single-step reaction (SSM: single-state model). In the following subsection this formalism is extended by considering a ligand binding induced conformational transition of the ligand–receptor complex (TSM: two-state model).

Single-State Model. It has been shown by Ortega (1988) that, for all ligands employed in the present study, the stoichiometry of binding to the $Fc_\epsilon RI$ is 1:1. Thus, the simplest reaction scheme for this process is

$$L + Fc \underset{k_{21}}{\overset{k_{12}}{\rightleftharpoons}} L\text{–}Fc \qquad (R1)$$

where L, Fc, and L–Fc represent the ligand, the $Fc_\epsilon RI$, and the $Fc_\epsilon RI$–ligand complex, respectively. The specific rates of ligand association and dissociation are denoted by k_{12} and k_{21}, respectively. The equilibrium concentration of bound ligand $[L]_b$ is calculated according to the mass action law:

$$[L]_b = K[L]_f[Fc]_f \qquad (1)$$

where K denotes the equilibrium constant and $[L]_f$, $[L]_b$, and $[Fc]_f$ are the concentrations of free and bound ligand and free receptor, respectively.

The concentrations of the free reactants are calculated by using the law of mass conservation, yielding the equation:

$$[Fc]_f = [Fc]_T - [L]_b \qquad (2a)$$

$$[L]_f = [L]_T - [L]_b \qquad (2b)$$

where $[Fc]_T$ and $[L]_T$ denote the total receptor and ligand concentrations. Inserting eqs 2a and 2b into eq 1, one obtains the concentration of bound ligand as a function of the total ligand concentration.

The general treatment of the kinetics of reaction R1 has to take into account that the $Fc_\epsilon RI$ resides in the cell membrane. Thus they are confined to a limited space, and rates of interactions with their ligands differ from those of reactants uniformly distributed in a homogeneous solution. Assuming the surface density of the receptor is relatively low—as is the case for mast cells and basophils (DeLisi, 1981)—the first collision of a ligand with a cell would most probably not be with a receptor, and therefore it would not form an encounter complex. However, since the cell's size is by far larger than that of the ligand, the latter can recollide with its surface, thus increasing the probability of forming an encounter complex. Hence the probability of forming ligand–receptor complexes depends on the free receptor density and the diffusion constant of the ligand. The dissociation probability of the ligand also depends on the free receptor concentration since a ligand that dissociates from one receptor may bind to an adjacent one prior to diffusing away from the cell. These events have been considered in detail by the theoretical treatments that derived concrete expressions for the association and dissociation rate constants of reaction R1 (Smoluchowski, 1917; Berg & Purcell, 1977; Shoup & Szabo, 1982; Goldstein et al., 1989):

$$k_{12} = 4\pi DRk_{on}/(4\pi DR + Nk_{on}) \qquad (3)$$

$$k_{21} = 4\pi DRk_{off}/(4\pi DR + Nk_{on}) \qquad (4)$$

where R denotes the radius of the cell, D is the diffusion coefficient of the ligand, N is the number of free receptors per cell, and k_{on} and k_{off} are the intrinsic association and dissociation rate constants expressed in units of $cm^3/(\text{cell Fc·s})$ and $(\text{cell Fc·s})^{-1}$, respectively.

The rate constants in eqs 3 and 4 do not depend on the receptor concentration if $4\pi DR \gg Nk_{on}$. This relation is valid when the binding process is limited by the actual reaction and not by diffusion. As shown later, this holds for all reagents (IgE, Fab-H10, Fab-J17, and Fab-F4) used. Therefore, the kinetics of reaction R1 can be described in terms of the differential equation:

$$d[L]_b/dt = k_{12}[Fc]_f(t)[L]_f(t) - k_{21}[L]_b(t) \qquad (5)$$

where the rate constants k_{12} and k_{21} are now expressed in units of $M^{-1}\ s^{-1}$ and s^{-1}, respectively. The solution of eq 5 is given in Appendix 1.

In this study we have also performed dissociation experiments by adding a large excess of unlabeled IgE to inhibit the reassociation of the labeled ligands. The corresponding reaction scheme is then

$$I + Fc \underset{k^I_{21}}{\overset{k^I_{12}}{\rightleftharpoons}} I\text{–}Fc \qquad (R2)$$

The inhibitor (I) association and dissociation rate constants are denoted by k^I_{12} and k^I_{21}, respectively. The rate equations for the combined reactions R1 and R2 are written as

$$d[L]_b(t)/dt = k_{12}[Fc]_f(t)[L]_f(t) - k_{21}[L]_b(t) \qquad (6a)$$

$$d[Fc]_f(t)/dt = -\{k_{12}[L]_f(t) + k^I_{12}[I]_f(t)\}[Fc]_f(t) + k_{21}[L]_b(t) + k^I_{21}[I]_b(t) \qquad (6b)$$

$$d[I]_b(t)/dt = k^I_{12}[Fc]_f(t)[I]_f(t) - k^I_{21}[I]_b(t) \qquad (6c)$$

If one adds a large excess of unlabeled IgE to the sample, practically all receptors are occupied by the inhibitor at the end of the dissociation process. For this case, calculation yields the following equation for $[L]_b(t)$:

$$[L]_b(t) = [Fc]_T + [Fc]_{f0}\exp(-\tau_2 t) + \alpha\{\exp(-\tau_1 t) - \exp(-\tau_2 t)\} \qquad (7)$$

where

$$\alpha = \frac{\tau_1\{\tau_2[Fc]_T - k^I_{12}[I]_f[Fc]_{f0}\}}{(\tau_1 - \tau_2)k^I_{12}[I]_T}$$

and $[Fc]_{f0}$ is the initial concentration of free $Fc_\epsilon RI$ sites. The time constants τ_1 and τ_2 are obtained from the secular equation:

$$\begin{vmatrix} k_{12}[L]_T - \tau_{1,2} & -k_{21} \\ -(k_{12} - k^I_{12})[L]_T k_{21} & -\tau_{1,2} \end{vmatrix} = 0 \qquad (8)$$

Equations 7 and 8 are used to describe the dissociation of labeled ligands in the presence of unlabeled IgE.

Two Conformational States Model. We now consider a ligand-induced conformational transition of the $Fc_\epsilon RI$–ligand complex. The corresponding reaction scheme is

$$L + Fc \underset{k_{21}}{\overset{k_{12}}{\rightleftharpoons}} (L\text{–}Fc)_l \underset{k_{32}}{\overset{k_{23}}{\rightleftharpoons}} (L\text{–}Fc)_h \qquad (R3)$$

where (L–Fc) denotes the initial low-affinity state l of the $Fc_\epsilon RI$–ligand complex and $(L\text{–}Fc)_h$ represents the $Fc_\epsilon RI$–ligand complex in the high-affinity state h. The concentration of bound ligand is now given by

$$[L]_b = K(K_c + 1)[Fc]_f[L]_f \qquad (9)$$

where $K = k_{12}/k_{21}$ and $K_c = k_{23}/k_{32}$ denote the equilibrium

constants of the first and the second reaction steps, respectively. Molar concentrations are used throughout. It can be seen by comparing eq 9 with eq 1 that reaction R3 can be described by an effective equilibrium constant $K_{eff} = K(K_c + 1)$.

Binding of the competing unlabeled IgE can be described by an analogous scheme to reaction R3, where the corresponding rate constants are denoted by k^I_{12}, k^I_{21}, k^I_{23}, and k^I_{32} for the two reaction steps and the equilibrium constants K^I and K_c^I.

The entire system is described by the following set of coupled nonlinear differential equations:

$$d[L]_{b1}(t)/dt = k_{12}[Fc]_f(t)[L]_f(t) - (k_{21} + k_{23})[L]_{b1} + k_{23}[L]_{b2} \quad (10a)$$

$$d[L]_{b2}(t)/dt = k_{23}[L]_{b1}(t) - k_{32}[L]_{b2}(t) \quad (10b)$$

$$d[Fc]_f(t)/dt = -\{k_{12}[L]_f(t) + k^I_{12}[I]_f(t)\}[Fc]_f(t) + k_{21}[L]_{b1}(t) + k^I_{21}[I]_{b1}(t) \quad (10c)$$

$$d[I]_{b1}(t)/dt = k^I_{12}[Fc]_f(t)[I]_f(t) - (k^I_{21} + k^I_{23})[I]_{b1}(t) + k^I_{23}[I]_{b2} \quad (10d)$$

$$d[dI]_{b2}(t)/dt = k^I_{23}[I]_{b1}(t) - k^I_{32}[I]_{b2}(t) \quad (10e)$$

where $[L]_{bj}$ and $[I]_{bj}$ denote the concentrations of ligand and inhibitor bound to receptors in the conformation j ($j = 1$ for the l state and $j = 2$ for the h state). Equations 10a–e must be solved numerically by a detailed procedure, which is described in Appendix 2.

Materials and Methods

Cells. Rat mucosal mast cells of the secreting subline RBL-2H3 (Barsumian et al., 1981) were cultured in MEM containing 10% FCS, 2 mM glutamine, and antibiotics, at 37 °C, in a water-saturated atmosphere with 7% CO_2.

Production of Hybridomas. The preparation and characterization of the Fc_ϵRI-specific mAbs F4, H10, and J17 have been described earlier (Ortega et al., 1988). Briefly, the hybridomas were obtained by fusing spleen cells from mice immunized intraperitoneally with RBL-2H3 cells, with NSO myeloma cells (ratio 5:1), essentially as described by Eshhar (1985). Selection was done by testing supernatants of the emerging hybridomas for their capacity to induce RBL-2H3 cell secretion. Positive clones were selected, expanded, retested, and cloned by limiting dilution. The selected clones were grown in tissue culture for production of mAbs.

Production and Purification of mAbs. The mAbs F4 (IgG_1), J17 (IgG_1), and H10 (IgG_{2b}) were purified from hybridoma culture supernatants by affinity chromatography on protein A–Sepharose columns (Pharmacia, Sweden). The mAbs were eluted from the column with 0.2 M glycine, pH 2.9. The eluate was collected directly into tubes containing neutralizing 2M Tris buffer, pH 8.2, dialyzed against PBS, and stored frozen at −20 °C.

Fab fragments of the three mAbs were prepared by digestion with papain at a 1:50 w/w ratio, in 20 mM Tris buffer, pH 8.2, containing 0.1 mM dithiothreitol and 2 mM EDTA. Digestion was carried out for 2 h at 37 °C, after which iodoacetamide (10 mM) was added for 1 h at 0 °C. Fc fragments and undigested antibody were eliminated by passing the preparation twice through a protein A–Sepharose column. The Fab preparations did not contain intact or partially digested molecules, as judged both by SDS–PAGE stained with Coomasie Blue and by their inability to induce secretion from RBL-2H3 cells.

Mouse monoclonal IgE (IgELa2; Rudolph et al., 1981), specific for the DNP hapten, was purified from ascitic fluid by chromatography on DNP-BSA–Sepharose 4B columns.

Antibody concentrations were determined by their absorbance at 280 nm using an $OD^{0.1\%}_{280nm} = 1.4$. For conversion to molar concentrations, a MW of 50K was assumed for the Fab fragments of mAbs H10, F4, and J17, and of 180K for intact IgE.

Fab fragments, or affinity-purified mouse IgE, were iodinated with ^{125}I by using the chloramine T method (Hunter & Greenwood, 1962). Specific activities in the range of 5–10 μCi/μg of protein were usually employed. After iodination, the labeled proteins were kept at 4 °C and used within 2–3 weeks.

Measurements of Interaction Rates. In order to ascertain the cells' viability during the relatively long (up to 8 h) times of some experiments, all measurements of the rates of binding or dissociation were carried out with the cells suspended in MEM containing 10% FCS and 20 mM HEPES, pH 7.4. Temperature was controlled by keeping the cell suspensions in thermostated water baths.

Association rates were measured by adding ^{125}I-labeled IgE or Fab fragments of the respective mAbs to cell suspensions [usually at (2–4) × 10^6 cells/mL], preequilibrated at the specified temperature. The samples were thoroughly mixed, and at the indicated times, three aliquots of 150 μL were taken, layered on 200 μL of FCS in microfuge tubes, and immediately centrifuged for 20 s in a Beckman microfuge. Each tube was cut and the radioactivity of its bottom, containing the cell pellet, was counted in a γ counter.

For measuring the dissociation rates, cell suspensions [(10–20) × 10^6 cells/mL] were incubated with the labeled ligands for 1–2 hours, in order to reach equilibrium. Dissociation was then initiated by diluting the cell suspensions (usually 1:10, but sometimes less) with medium containing the indicated concentrations of unlabeled IgE. At the given times, three aliquots of 150 μL were transferred into microfuge tubes containing 200 μL of FCS and centrifuged immediately for 20 s. The tubes were cut, and the bottoms containing the cell pellets were counted to determine the remaining bound ligand. The concentration of bound ligand at the start of the experiment (time = 0) was determined on samples taken from the original cell suspension immediately before dilution and processed by the same protocol.

The molar concentration of available Fc_ϵRI sites in each association and dissociation experiment was determined by incubating cell samples with a saturating concentration of ^{125}I-labeled IgE or Fab-H10 (usually at 5 × 10^{-8} M) for at least 2 h and measuring the bound probe as before. Correction for nonspecific binding was done by subtracting the radioactivity found associated with similar cell samples that were preincubated with >10^{-6} M unlabeled IgE for 1 h before addition of the labeled ligand.

At the end of each experiment, the cell number in each suspension, used for either ligand binding kinetics or for determining Fc_ϵRI concentration, was directly determined by cell counting under the microscope. Variation among samples was minimal (less than 5%), and thus no correction was necessary. No noticeable cell damage was evident upon microscopic examination, yet in some experiments cell viability was checked also by Trypan blue exclusion and found to be >90% at the end of the measurements.

Fitting Procedure. Equation A1.3 of Appendix 1 and eq 7 were employed to fit the association and dissociation rates with the SSM. In this procedure, the specific rates k_{12} and k_{21} were used as the free parameters. The fitting to the TSM was carried out by employing an interactive procedure in-

Table I: Kinetic Parameters of the Interaction between Specific Ligands with $Fc_\epsilon RI$ on RBL-2H3 Cells[a]

ligand	temp (°C)	expt[b]	k_{12}[d] (M^{-1} s^{-1})	k_{21} (s^{-1})	k_{23} (s^{-1})	k_{32} (s^{-1})	k_{23}/k_{21}	model[c]
Fab-J17	25.0	A	4.0×10^5	1.9×10^{-2}				1
	25.0	A	3.0×10^5	1.2×10^{-2}				1
	25.0	A	3.3×10^5	2.1×10^{-2}				1
	25.0	D	2.4×10^5	1.5×10^{-2}	8.0×10^{-5}	1.5×10^{-3}		2
	25.0	D	2.8×10^5	1.2×10^{-2}	5.5×10^{-2}	1.0×10^{-3}		2
	25.0	D	2.8×10^5	1.2×10^{-2}	8.0×10^{-5}	1.5×10^{-3}		2
	25.0	D	2.8×10^5	1.2×10^{-2}	8.0×10^{-5}	1.5×10^{-3}		2
	15.0	A	4.5×10^5	1.5×10^{-2}	5.0×10^{-4}	1.5×10^{-3}		2
	15.0	D	4.3×10^5	1.8×10^{-2}	6.0×10^{-4}	9.0×10^{-3}		2
	4.0	A	3.5×10^5	1.0×10^{-2}	8.0×10^{-4}	1.0×10^{-3}		2
	4.0	D	1.1×10^5	6.0×10^{-3}	1.0×10^{-3}	6.0×10^{-4}		2
Fab-F4	25.0	A	5.0×10^4	5.3×10^{-3}				1
	25.0	A	2.1×10^4	8.0×10^{-3}				1
	25.0	A	8.0×10^4	5.5×10^{3}				1
	25.0	A	5.5×10^4	4.2×10^{-3}				1
	25.0	D	6.3×10^4	7.0×10^{-3}	2.0×10^{-4}	1.0×10^{-3}		2
	25.0	D	9.1×10^4	7.0×10^{-3}	2.4×10^{-4}	1.0×10^{-3}		2
	25.0	D	7.0×10^4	7.0×10^{-3}	2.1×10^{-4}	1.0×10^{-3}		2
	25.0	D	6.5×10^4	5.0×10^{-3}	2.1×10^{-4}	6.0×10^{-4}		2
	15.0	A	5.0×10^4	5.0×10^{-3}	5.0×10^{-4}	5.0×10^{-4}		2
	15.0	D	4.5×10^4	7.0×10^{-3}	5.0×10^{-4}	6.0×10^{-4}		2
	4.0	A	4.0×10^4	7.0×10^{-3}	1.4×10^{-3}	3.0×10^{-4}		2
	4.0	D	3.0×10^4	7.0×10^{-3}	5.0×10^{-4}	6.0×10^{-4}		2
Fab-H10	25.0	A	2.3×10^5	1.6×10^{-3}				1
	25.0	A	2.3×10^5			1.0×10^{-2}	32	2
	25.0	D	1.4×10^5			1.0×10^{-2}	40	2
	25.0	D	1.0×10^5			2.0×10^{-2}	43	2
	25.0	D	1.0×10^5			1.4×10^{-2}	46	2
	15.0	A	1.0×10^5			9.5×10^{-3}	30	2
	15.0	D	5.0×10^4			3.0×10^{-2}	84	2
	4.0	A	5.0×10^4			4.0×10^{-3}	125	2
	4.0	D	1.5×10^4			1.1×10^{-2}	55	2
IgE	25.0	A	7.1×10^4	2.0×10^{-4}				1
	25.0	A	5.3×10^4	2.3×10^{-4}				1
	25.0	A	2.7×10^4	4.5×10^{-4}				1
	25.0	A	7.0×10^4			4.0×10^{-3}	66	2
	25.0	A	4.0×10^4			4.0×10^{-3}	66	2
	25.0	D	1.0×10^4			5.0×10^{-3}	58	2
	25.0	D	1.2×10^4			4.5×10^{-3}	30	2
	25.0	D	1.0×10^4			5.5×10^{-3}	46	2
	15.0	A	2.8×10^4			2.5×10^{-3}	32	2
	15.0	D	1.0×10^4			7.0×10^{-3}	86	2
	4.0	A	9.0×10^3			2.0×10^{-3}	200	2
	4.0	D	6.6×10^3			5.0×10^{-3}	71	2

[a] Each set of parameters (one line of the table) was derived from experiments performed on different cell batches. Thus each dissociation experiment consisted of at least one DCD and one DCDI, which were fitted with the same parameter values. Likewise, some of the individual association experiments included ACs measured at two different ligand concentrations which were fitted with the same parameter values. [b] A = measurement of association rates, D = measurement of dissociation rates. [c] Model used to derive the parameters included in the table. 1 = SSM, 2 = TSM. [d] Standard deviation of the values for the rate constants is in the range between 10% and 30%.

volving eq A2.2–A2.5 of Appendix 2. When the data obtained with the Fabs of J17 and F4 were fitted, the specific rates k_{12}, k_{21}, k_{23}, and k_{32} were used as free parameters. For reasons explained under Results, for fitting the IgE and Fab-H10 data to the TSM, we had to use the values of k_{12}, k_{32}, and k_{23}/k_{21} as the free parameters. The computer fitting procedure employed the program MINUITL (CERN library; James & Ross, 1975), which contains several different minimizing subroutines enabling the search for a local minimum in the χ^2 function between the experimental data and the computed values.

Results

The association and dissociation rates of IgE and the Fab fragments of the $Fc_\epsilon RI$-specific mAbs, F4, J17, and H10 with and from $Fc_\epsilon RI$ on living RBL-2H3 cells were measured at the three temperatures: 25, 15, and 4 °C. Association or dissociation of all four ligands was usually measured in parallel on cells taken from the same batch. The association experiments are labeled as ACs and the dissociation experiments as DCD (dissociation by dilution) and DCDI (dissociation by dilution and unlabeled IgE) throughout this paper. For reasons of clarity, we present first the analysis of the IgE association and dissociation and later proceed to the analysis of the Fab data.

Kinetics of IgE binding (25 °C). The kinetic analysis of $Fc_\epsilon RI$–IgE interactions is presented first as the rate constants of IgE binding are required for treatment of the DCDI experiments (eqs 10a–e).

The association of IgE was measured at several different IgE concentrations. Results are illustrated in the lower panel of Figure 1. In a first approach, these data were analyzed according to the simplest scheme, i.e., the SSM (eq 5). Both ACs were fitted (full lines in Figure 1) by using the very same k_{12} and k_{21} values listed in Table I. This was achieved at different receptor occupation: at one of the IgE concentrations employed, close to 90% saturation of the $Fc_\epsilon RI$s was obtained, while only 25% saturation was reached in the other one. Both experiments were done on the same batch of cells. This clearly shows that the rate constants are independent of the free receptor density on the cell surface, in accordance with the applied theory [cf. Theory, Berg and Purcell (1977), and DeLisi (1980, 1981)]. This observation is also in full agreement with the previously published results of Wank et al. (1983). It should be noted that the data allow a rather precise

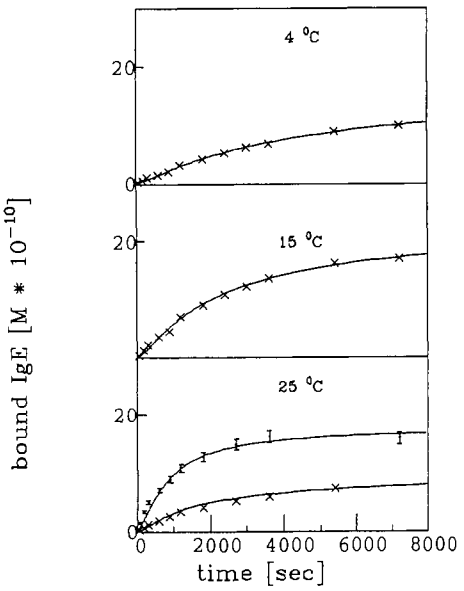

FIGURE 1: Time course of ^{125}I-IgE association to cell resident $Fc_\epsilon RI$ measured at 25 °C (lower panel), 15 °C (intermediate panel), and 4 °C (upper panel). ^{125}I-IgE was added to cell suspension (2.5×10^6 cells/mL) precquilibrated at the respective temperature. After the indicated time, the bound radioactive protein was measured as described under Materials and Methods. The ligand concentrations were adjusted to 1.2×10^{-8} M (•) and 3.0×10^{-9} M (×) for the measurements at 25 °C, and to 5.5×10^{-9} M at 15 and 4 °C. The $Fc_\epsilon RI$ concentration was 1.9×10^{-9} M at 25 °C and 4.2×10^{-9} M at 15 and 4 °C. The solid lines results from the fit to the data. The error bars in the lower panel illustrate the statistical error of the data displayed in all panels.

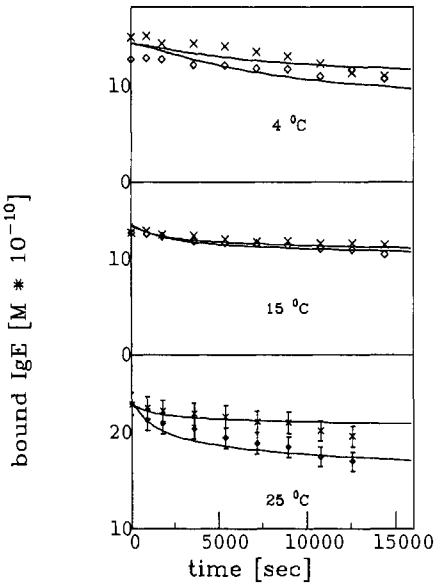

FIGURE 2: Time course of ^{125}I-IgE dissociation from $Fc_\epsilon RI$ on RBL-2H3 cells in the presence (◊: 7×10^{-7} M) and absence (×) of unlabeled IgE measured at 25 °C (lower panel), 15 °C (intermediate panel), and 4 °C (upper panel). Cells (2.5×10^6 cells/mL) were incubated with ^{125}I-IgE for 2 h at the respective temperature. Dissociation was initiated by 1:10 dilution of the cell suspensions with medium with (◊) or without (×) unlabeled IgE. At the indicated time, the amount of bound ^{125}Ig-IgE was measured as described under Materials and Methods. The concentration of labeled IgE was adjusted to 2.0×10^{-8} M at 25 °C and to 2.8×10^{-8} M at 15 and 4 °C. The $Fc_\epsilon RI$ concentration was 3.08×10^{-8} M (25 °C) and 2.25×10^{-8} M (15 and 4 °C) before dilution. The lines result from fitting of the data to the TSM. The data on all panels show statistical errors similar to those showed in the lower panel.

derivation of the rate constants. While the association rate constant is determined by the linear slope of the initial phase, the dissociation rate constant affects the deviation from the linear slope, i.e., the intermediate and the plateau region of the AC. Thus, the experimental error indicated by the bars also provides a measure of the accuracy of the derived rate constants (maximum 10%).

IgE association experiments were also performed on several different cell batches. While their analysis yielded quite similar dissociation rate constants, the derived association rate constants exhibited a larger scatter, but were all in the same order of magnitude (Table I). From the k_{12}/k_{21} ratios (Table I), one derives a value for the equilibrium constant which is 3–5 times larger than that obtained from equilibrium binding studies carried out on the same cell batch and at the same temperature (Ortega et al., 1988). This discrepancy may be due to the fact that IgE binding equilibrium is not attained after an incubation time of 1 h (Figure 1, lower panel), which was employed for the binding studies. Therefore, in this study, all dissociation experiments of labeled IgE were carried out after an incubation time of at least 2 h.

In view of the observation that the rate constants of IgE binding are not affected by the free receptor density, the dissociation rate constant derived from the ACs in Figure 1 can be used for the analysis of both types of dissociation experiments, namely, the DCD and the DCDI. Figure 2 (lower panel) displays results of an IgE DCD and an IgE DCDI experiment using the same batch of cells and the same concentration of ^{125}I-IgE. In these experiments, dissociation was initiated after a 2-h incubation time. Inspection of the IgE dissociation data shows that it proceeds rather slowly as compared to the association. Thus, assuming a single-step equilibrium, one calculates, from the slope of the DCs, a dissociation rate of 1.0×10^{-5} s^{-1}, a value that is only slightly larger than that derived by Wank et al. (1983). This value, however, is 20–40-fold smaller than the dissociation rate constants emerging from the analysis of the association data described above (Table I). This discrepancy suggested that IgE binding cannot be described consistently in terms of the SSM.

The results of applying the TSM (eqs 10a–e and A2.3) to the DCD and DCDI data are displayed in the lower panel of Figure 2. Good fits to the experimental data are obtained (solid lines). Both DCD and DCDI were fitted in terms of the very same parameter values. These values were also used to account for the binding of the unlabeled IgE which inhibited reassociation. These results demonstrate that the two-state model can be used to reconcile the IgE DCD and DCDI in an internally consistent manner. It should be mentioned, however, that not all rate constants of the two-step process can be derived from this analysis. This is caused by the large, inherent correlation effects between k_{23} (forward rate constant of the conformational transition) and k_{21} (dissociation rate constant). These correlation effects occur when k_{23} and k_{21} are in the same order of magnitude. In this case, a decrease in k_{21} and an increase in k_{23} affect the fits in a similar manner. We therefore used the ratio k_{23}/k_{21} as a parameter in the fit. The reverse rate constant k_{32} is derived from the fit to the DCDI, whereas the association rate constant k_{12} is obtained from the fit to the DCD. We also applied the TSM to two further sets of DCDs and DCDI measurements carried out on different cell batches. The derived rate constants are similar to the values emerging from the analysis of the data shown in Figure 2. The parameter values for the various experiments are listed in Table I.

The large k_{23}/k_{21} ratio observed indicates that the dissociation of the ligand–receptor complex l proceeds much slower than its conversion into the second conformation h. In order

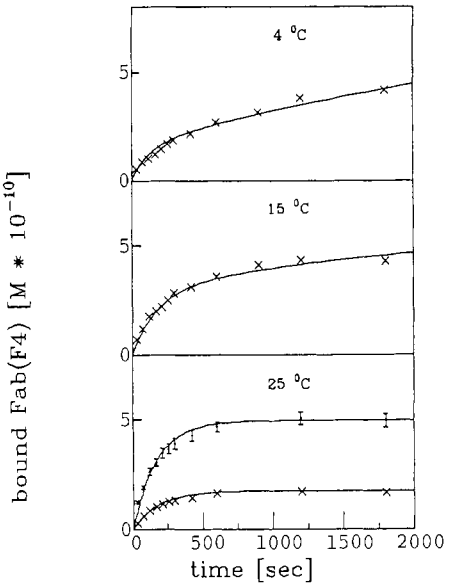

FIGURE 3: Time course of ^{125}I-Fab-F4 association to cell resident Fc$_\epsilon$RI measured at 25 °C (lower panel), 15 °C (intermediate panel), and 4 °C (upper panel). Experimental details are similar to those for Figure 1. ^{125}I-Fab-F4 concentration was adjusted to 1.2×10^{-8} M (•) and to 4.1×10^{-9} M (×) for the measurement at 25 °C and to 8.4×10^{-9} M at 15 and 4 °C. The Fc$_\epsilon$RI concentration was 4.8×10^{-9} M at 25 °C and 4.2×10^{-9} M at 4 °C. The lines result from the fit of the data to the SSM. The data in all panels show statistical error similar to that show in the lower panel.

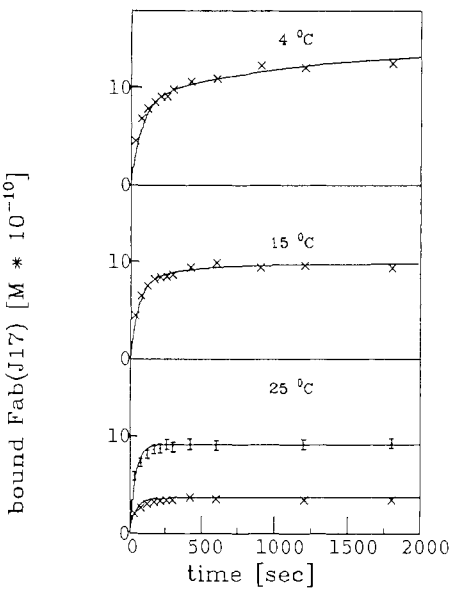

FIGURE 4: Time course of ^{125}I-Fab-J17 association to cell resident Fc$_\epsilon$RI measured at 25 °C (lower panel), 15 °C (intermediate panel), and 4 °C (upper panel). Experimental details are similar to those for Figure 1. ^{125}I-Fab-J17 concentration was adjusted to 1.2×10^{-8} M (•) and to 3.9×10^{-9} M (×) for the measurement at 25 °C and to 2.7×10^{-9} M at 15 and 4 °C. Fc$_\epsilon$RI concentration was 4.8×10^{-9} M at 25 °C and 4.2×10^{-9} M at 4 °C. The lines result from the fit to the data. The data in all panels show statistical error similar to that show in the lower panel.

to determine whether the ACs shown in Figure 1 agree with the two-state model, we used eqs A2.2–A2.5 to fit the experimental data, allowing again k_{23}/k_{21}, k_{32}, and k_{12} to be the free parameters. Both ACs could be fitted by using the very same parameter values (Table I). The fitted curves are rather close to those of the SSM (data not shown). Hence, we conclude that the TSM is the simplest mechanism that can satisfactorily describe all the association and dissociation interactions of IgE and the Fc$_\epsilon$RI in a complete and internally consistent way. We further suggest that the rate constants obtained from the fit of the ACs to the SSM (Table I) have to be regarded only as effective parameters averaging over the contributions of the two reaction steps. Therefore, they cannot be related to respective steps of the binding process. Under Discussion, we will show that the TSM can also be used to describe the kinetic data of Fc$_\epsilon$RI–IgE interaction measured by Wank et al. (1983).

Binding Kinetics of H10-, J17-, and F4-Fab Fragments (25 °C). The ACs of Fab fragments of the three different Fc$_\epsilon$RI-specific mAbs are presented in the lower panels of Figures 3–5. Application of the SSM (eq 5) to these data yielded good fits as illustrated by the solid lines in the corresponding figures. Again, the ACs of each ligand obtained over a range of its concentrations could be fitted by using the same values for the association and dissociation rate constants. This shows that the interaction kinetics of these ligands are also independent of the free receptor concentration (Berg & Purcell, 1977; DeLisi, 1980). The rate constants derived from the fits are listed in Table I. Further experiments, using two different cell batches, yielded very similar results (Table I). It is noteworthy that the equilibrium constants K calculated from the ratios of the respective rate constants are in good agreement with those derived from previous equilibrium studies [cf. Ortega et al. (1988)]. Further, while the equilibrium binding constants of Fab-J17 and Fab-F4 are nearly identical, the specific rates of association and dissociation of Fab-J17 are considerably faster than those of Fab-F4.

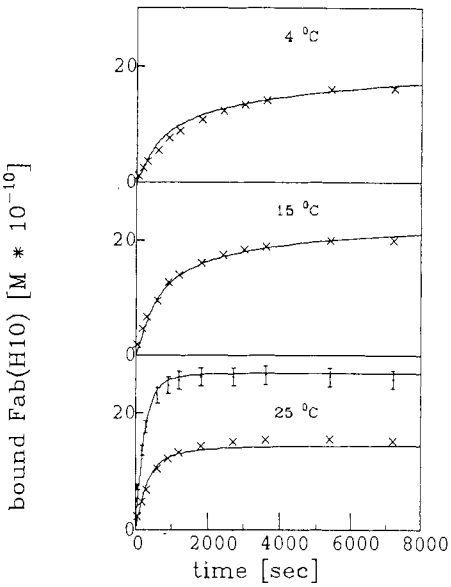

FIGURE 5: Time course of ^{125}I-Fab-H10 association to cell resident Fc$_\epsilon$RI measured at 25 °C (lower panel), 15 °C (intermediate panel), and 4 °C (upper panel). Experimental details are similar to those for Figure 1. ^{125}I-Fab-H10 concentration was adjusted to 1.1×10^{-8} M (•) and to 3.7×10^{-9} M (×) for the measurement at 25 °C and to 2.7×10^{-9} M at 15 and 4 °C. The Fc$_\epsilon$RI were at a concentration of 4.8×10^{-9} M at 25 °C and of 4.2×10^{-9} M at 4 °C. The solid lines results from the fit to the data. The data in all panels show statistical error similar to that shown in the lower panel.

DCD and DCDI of the Fab fragments of F4, J17, and H10 were determined. While the SSM can describe the association of the three Fabs, it does not yield satisfactory fits to the dissociation data of any of them. Moreover, semilogarithmic plots of the DCDs and DCDIs are biphasic (Figures 6–8), suggesting the existence of a second step in the dissociation process. These findings suggest that the TSM should also be used to analyze the kinetics of the interaction between the Fabs and the Fc$_\epsilon$RI. Hence we employed eqs A2.2–A2.5 to fit the

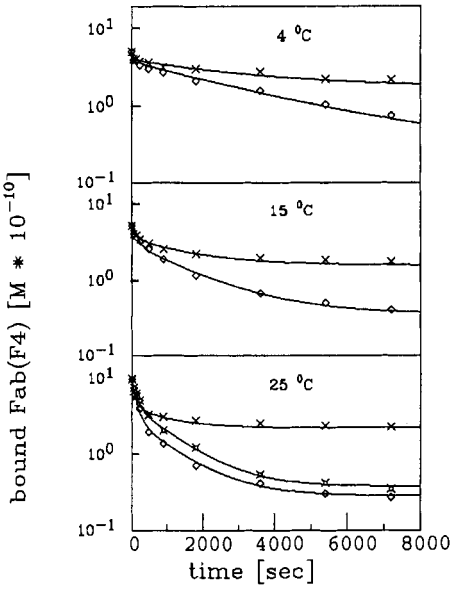

FIGURE 6: Time course of ^{125}I-Fab-F4 dissociation from Fc_ϵRI on RBL-2H3 cells in the presence of 4×10^{-7} M (◊), 1×10^{-8} M (⊠), or absence (×) of unlabeled IgE measured at 25 °C (lower panel), 15 °C (intermediate panel), and 4 °C (upper panel). Experimental procedures were similar to those for Figure 2. Concentration of ^{125}I-Fab-F4 was adjusted to 7.0×10^{-8} M at 25 °C and to 5.6×10^{-8} M at 15 and 4 °C. The receptors were at a concentration of 3.1×10^{-8} M (25 °C) and 2.3×10^{-8} M (15 and 4 °C) before dilution. The lines result from fitting the TSM to the data. The statistical errors of each data set are smaller than the size of the respective symbols.

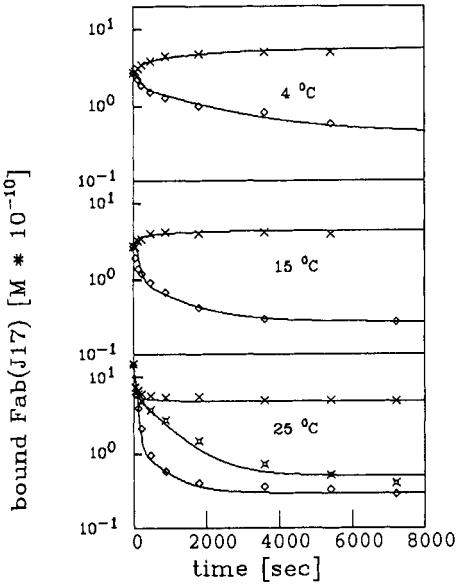

FIGURE 7: Time course of ^{125}I-Fab-J17 dissociation from Fc_ϵRI on RBL-2H3 cells in the presence of 4×10^{-7} M (◊), 1×10^{-8} M (⊠), or absence (×) of unlabeled IgE, measured at 25 °C (lower panel), 15 °C (intermediate panel), and 4 °C (upper panel). Experimental procedures were similar to those for Figure 2. The concentration of labeled Fab-J17 was adjusted to 6.7×10^{-8} M at 25 °C and to 5.4×10^{-8} M at 15 and 4 °C. The receptors were at a concentration of 3.1×10^{-8} M (25 °C) and 2.3×10^{-8} M (15 and 4 °C) before dilution. The lines result from fitting the TSM to the data. The statistical errors of each data set are smaller than the size of the respective symbols.

data. As shown in the lower panels of Figures 6–8, excellent agreement with all data sets is obtained. Again, we fit the corresponding DCDs and DCDIs of each ligand using one common set of rate constant values. To describe the interactions of unlabeled IgE, we used a representative set of the rate constants listed in Table I. Because of the low values of the k_{23}/k_{21} ratios, the determination of k_{23} and k_{21} for Fab-J17

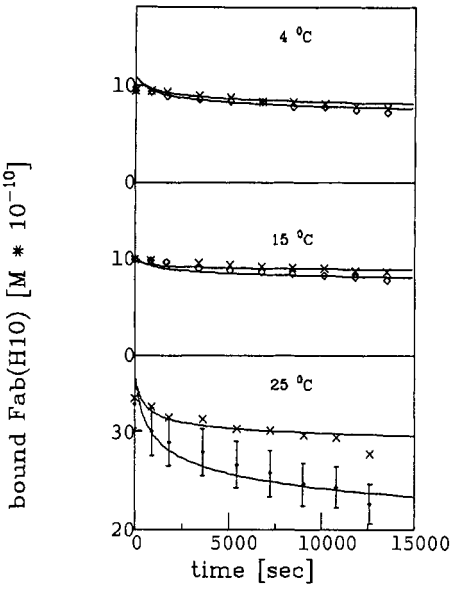

FIGURE 8: Time course of ^{125}I-Fab-H10 dissociation from Fc_ϵRI on RBL-2H3 cells in the presence of (◊: 4×10^{-7}M) and absence (×) of unlabeled IgE measured at 25 °C (lower panel), 15 °C (intermediate panel), and 4 °C (upper panel). Experimental procedures were similar to those for Figure 2. The concentration of labeled H10 was adjusted to 2.7×10^{-8} M at 25 °C and to 2.6×10^{-8} M at 15 and 4 °C. The receptors were at a concentration of 3.1×10^{-8} M (25 °C) and 2.3×10^{-8} M (15 and 4 °C) before dilution. The lines result from fitting the TSM to the data. The error bars in the lower panel represent practically the statistical error of the data displayed in all three panels.

and Fab-F4 is not affected by correlation effects. Further dissociation rate measurements were performed by using two different cell batches. Analysis of these further confirmed the conclusions reached on the basis of the data shown in Figures 6–8. All the best fit values derived from different experiments are listed in Table I.

Comparison of association and dissociation data for all ligands indicates that, due to the low values of K_c, the ACs and the equilibrium constants of Fab-F4 and Fab-J17 remain nearly unaffected by the second step. In contrast, for Fab-H10, $K_c \gg 1$, and hence the transition into the second state affects significantly the time course of association. Therefore, one has to use the two-state model to describe the Fab-H10 ACs. The values obtained are in good agreement with those derived from the dissociation data sets. In this case the fitted curve is nearly identical with that resulting from the fit to the single-state model. This shows that the rate constants derived from the ACs of Fab-H10 by means of the SSM must be regarded as effective ones, similar to what has been determined for IgE association. The consistency between the rate constant values derived from the association and dissociation processes deserves further comment; while for Fab-J17 and Fab-F4 all rate constants obtained from the DCDIs and DCDs are reproduced by the respective parameters derived from the ACs, the association rates of H10 and IgE suggest that k_{12} values are systematically larger than those derived from analysis of the corresponding dissociation rates (cf. Table I). This discrepancy cannot be related to uncertainties of the fitting procedure, because the DCDs are very sensitive even to small changes of k_{12}. It can be explained, however, if one takes into account that the ligand concentration used in the dissociation experiments is lower for IgE and H10 (2×10^{-8} M and 2.7×10^{-8} M at 25 °C) than for F4 and J17 (7×10^{-8} M and 6.7×10^{-8} M at 25 °C). Hence, dilution by a factor of 10 yields equilibrium concentrations for the bound ligands which for J17 and F4 are still in the saturation region of the cor-

Table II: Activation Enthalpies and Entropies As Derived from the Arrhenius Plots of the Rate Constants k_{ij}

	ΔH_{12} (kJ/M)	ΔH_{21} (kJ/M)	ΔH_{23} (kJ/M)	ΔH_{32} (kJ/M)
J17	6.1	14.1	−78.9	13.2
F4	3.5	0.6	−54.8	35.3
H10	46.5			26.5
IgE	59.0			9.1
	ΔS_{12} [kJ/(M·K)]	ΔS_{21} [kJ/(M·K)]	ΔS_{23} [kJ/(M·K)]	ΔS_{32} [kJ/(M·K)]
J17	−0.13	−0.31	−0.52	−0.21
F4	−0.10	−0.25	−0.61	−0.28
H10	0.006			−0.21
IgE	0.068			−0.24

responding binding isotherms [cf. Ortega et al. (1988)]. For H10 and IgE, however, the equilibrium is shifted to the increasing phase of the binding process. Thus variations of the initial ligand concentration caused by some inherent uncertainties of the dilution process yield a variation especially of the DCDs of H10 and IgE but do not affect the dissociation data of J17 and F4. Since the determination of k_{12} depends of the concentration of bound ligands in a nonlinear way, even a small variation of the DCD may cause significant changes in k_{12}.

It becomes evident from the results presented in this subsection that the TSM is the minimal reaction scheme required to provide a consistent fit to both the association and the dissociation data of four examined monovalent $Fc_\epsilon RI$ ligands: IgE and Fab fragments of J17, F4, and H10.

Determination of the Activation Barriers. In order to further characterize the $Fc_\epsilon RI$–ligand interaction, we measured the association and dissociation of the four ligands also at two lower temperatures (4 and 15 °C). Applying the above-described TSM, a consistent description of the corresponding data sets was achieved, as demonstrated by the lines in Figures 3–5 (association data) and in Figures 6–8 (dissociation data). The parameter values obtained are listed in Table I. The relatively high values of K_c for Fab-H10 and IgE do not enable the determination of the specific rate of k_{21} and k_{23} from the data.

It is noteworthy that, due to the increase in K_c with decreasing temperature, the association rates of Fab-J17 and Fab-F4 are also affected by the conformational transition of the ligand–receptor complex. Hence, in contrast to the situation encountered at 25 °C, the ACs of Fab-F4 and Fab-J17 cannot be fitted in terms of the SSM. At lower temperatures K_c exhibits intermediate values (K_c = 0.3–5.0) and the conformational transition proceeds at a slower rate than the receptor association with the ligands. This is reflected by the ACs in the following way: the initial phase is determined by the binding step, whereas the nearly linear increase in the concentration of bound ligands after ca. 1000 s is primarily determined by the conformational transition (cf. the intermediate and upper panels of Figures 3 and 4). The good fits to the ACs further corroborate the applicability of the TSM.

The enthalpic and entropic contributions to the activation barriers were derived from Arrhenius plots of the respective rate constants:

$$\ln k_{ij} = \ln \nu - 1/R(\Delta H_{ij}/T + \Delta S_i) \qquad (11)$$

where ΔH_{ij} and ΔS_{ij} ($i\,j$ = 1, 2, 3) are the corresponding enthalpy and entropy changes of the transition from state i to state j of reaction R3, whereas ν is a frequency factor for which a value of 10^{13} s^{-1} has been estimated for first-order reactions and of 10^{11} M^{-1} s^{-1} for second-order reactions (Austin et al., 1975). The Arrhenius plots are shown in Figure 9.

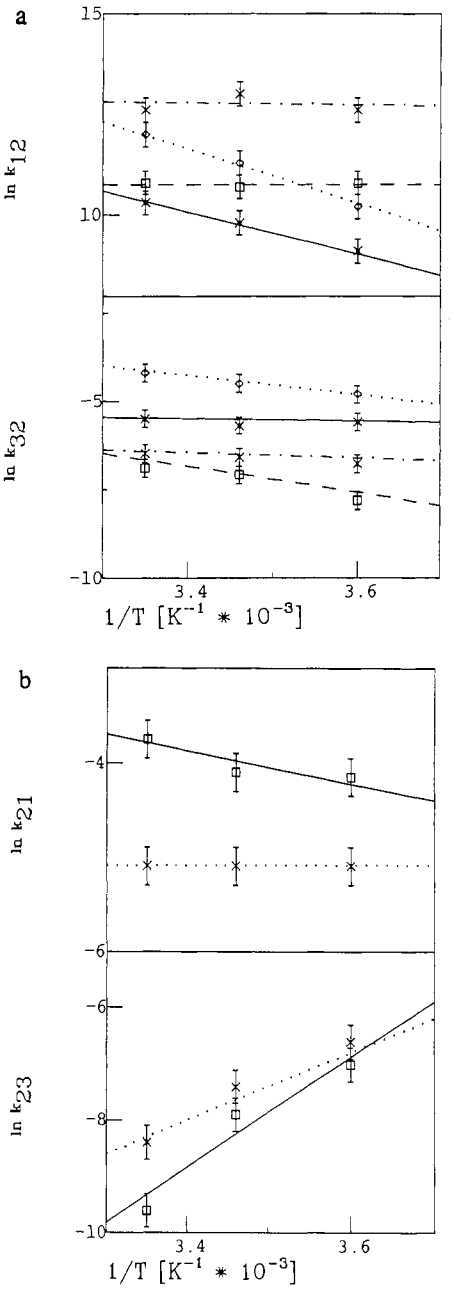

FIGURE 9: (a) Arrhenius plots of the rate constants k_{12} and k_{32}. The plots were obtained from the analysis of the association and dissociation data measured at 25, 15, and 4 °C: (◇) Fab-H10; (○) IgE; (×) Fab-J17; and (□) F4. The lines result from a fit to the data using eq 11. (b) Arrhenius plots of the rate constants k_{21} and k_{23}. The plots were obtained from the analysis of the association and dissociation data measured at 25, 15, and 4 °C: (×) Fab-J17 and (□) Fab-F4. The lines present the best fit to the data using eq 11.

From the fitting of eq 11 to the data, one calculates the activation enthalpy and entropy for each rate constant. These are listed in Table II.

The rate constants can be classified on the basis of their temperature dependence as follows: (1) The association rates k_{12} of Fab-F4 and Fab-J17 are nearly temperature independent, whereas those of Fab-H10 and IgE increase significantly with rising temperature. (2) The dissociation rate k_{21} of Fab-F4 is practically temperature independent, while that of Fab-J17 increases slightly with temperature. (3) The rate constant k_{23} of the l → h transition decreases significantly with rising temperature for both Fab-J17 and Fab-F4, whereas the rate constant for the reverse h → l transition (k_{32}) increases slightly for IgE and Fab-J17 and significantly for Fab-F4 and

Table III: Values of the Specific Rate Constants Derived from the Fit to the TSM of Six Association Experiments of IgE (Designated as A–F) and Various Receptor Concentrations Measured at 25 °C by Wank et al. (1983)

	$[F_c]_T$ (M)	k_{12} (M^{-1} s^{-1})	k_{32} (s^{-1})	k_{23}/k_{23}
A	1.55×10^{5}	1.2×10^{5}	2.0×10^{-3}	17
B	1.18×10^{-9}	1.2×10^{5}	2.0×10^{-3}	17
C	1.01×10^{-9}	1.0×10^{5}	2.0×10^{-3}	17
D	7.53×10^{-10}	1.1×10^{5}	2.0×10^{-3}	17
E	4.87×10^{-10}	1.1×10^{5}	2.0×10^{-3}	17
F	3.70×10^{-10}	1.1×10^{5}	2.0×10^{-3}	17

Fab-H10 with rising temperatures. This implies that the probability of the conformational transition decreases with rising temperature.

Discussion

The results presented here provide evidence that the binding of four different monovalent ligands—namely, IgE and Fab fragments of three $Fc_\epsilon RI$-specific mAbs—to the $Fc_\epsilon RI$ induces a conformational transition of the $Fc_\epsilon Ri$–ligand complex from a low-affinity state l to a high-affinity state h. The probability of inducing this conformational transition is different for each of the employed ligands. Earlier kinetic studies of IgE–$Fc_\epsilon RI$ interactions (Kulczycki & Metzger, 1976; Wank et al., 1983) suggested that it can be described by a single-step process. From measurements of the initial rates of binding and dissociation, the respective rate constants were calculated and their ratios were assumed to equal the equilibrium constant of the interaction. This yielded values as high as 10^{11} M^{-1}, considerably higher than those derived from equilibrium binding isotherms of IgE to the $Fc_\epsilon RI$ (Ishizaka et al., 1975; Ortega et al., 1988).

In order to clarify this discrepancy, the kinetics of interaction of four monovalent ligands with $Fc_\epsilon RI$ on RBL-2H3 cells were investigated over the temperature range of 4–25 °C. Analysis of the concentration and time dependencies of both association and dissociation, using the formalism derived from the SSM, has shown that the specific dissociation rate derived from the ACs of IgE is an order of magnitude higher than that obtained from the respective DCDs and DCDIs. Analysis of the data of Wank et al. (1983) shows that such a discrepancy can also be observed. In the latter study, the cells were reacted with a 2-fold excess of unlabeled IgE for various time periods prior to exposure to ^{125}I-IgE. This was done in order to provide different concentrations of free $Fc_\epsilon RI$. Thus six ACs designated as A–F were observed. If one now uses the rate constants reported by these authors in order to fit these data sets in terms of the SSM (reaction scheme R1 under Theory), one obtains a good fit to the AC designated as A and only to the initial phases of the remaining ACs (B–F). For the latter ones, however, the amount of bound ligand after 400 s is significantly overestimated. This is clearly shown for the ACs C–E by the dotted lines in Figure 10. We therefore examined whether the data of Wank et al. (1983) can be fitted to the TSM in an internally consistent manner. Indeed, a good fit of all these data sets was achieved (solid lines in Figure 10), yielding practically the same values for the respective rate constants. These are listed in Table III.

It should be noted that there are some differences between the rate constants derived by applying the TSM to the ACs of Wank et al. (1983) (Table III) and the values emerging from the analysis of our own data (Table I). The association rates derived from their data are larger by a factor of 2–3 than ours, whereas the k_{23} values resulting from the fits to their ACs are smaller by a factor of 2. These differences emerge from the experimental data and therefore do not depend on whether

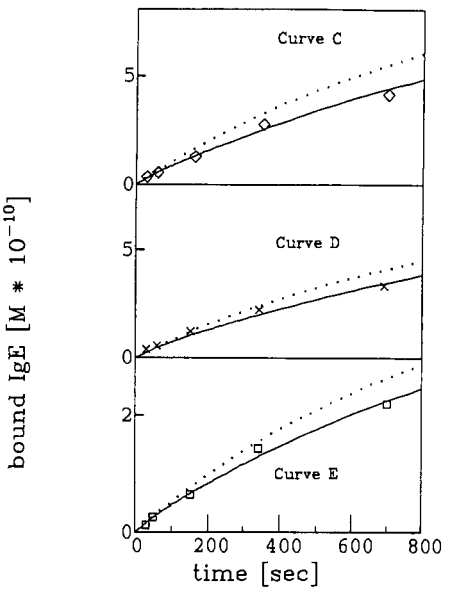

FIGURE 10: Association of ^{125}I-IgE to cells (2.3×10^{6} cells/mL) bearing variable numbers of unoccupied receptors. The data were taken from Wank et al. (1983), where the receptor concentration was adjusted by adding a 2-fold excess of unlabeled IgE to the cells for various periods of time prior to reaction with ^{125}I-IgE. The three association curves were determined at the following available receptor concentrations: curve C (◇), 1.0×10^{-9} M; curve D (×), 7.5×10^{-10} M; curve E (□), 4.9×10^{-10} M. The dotted lines are the results of a fit to the SSM using the kinetic parameters of Wank et al. (1983), whereas the fits to the TSM yield the solid lines.

one employs the SSM or TSM. They could be related to the different IgEs used: Wank et al. used rat IgE, while we used mouse IgE. In a previous study of the interaction rates of rat and mouse IgE with the $Fc_\epsilon RI$ on RBL cells, only slight differences were observed (Sterk & Ishizaka, 1982). While such small differences can contribute to the discrepancy, other experimental parameters could also be important.

The possibility that internalization of the bound ligands might take place and thus compromise the validity of our analysis also needs to be considered. A number of reasons make this possibility rather unlikely: It has been shown that unaggregated $Fc_\epsilon RI$–IgE complexes remain on the cell surface for periods of at least 19 h (Isersky et al., 1979), much longer than the time length of any of our experiments. Moreover, the fact that, in the presence of excess unlabeled IgE, >95% of the bound J17-Fab and F4-Fab are found to dissociate strongly suggests that practically all the $Fc_\epsilon RI$–Fab complexes remain on the cell surface. Finally, internalization of receptor–ligand complexes is expected to be greatly inhibited at 4 °C. This is the case even for aggregated $Fc_\epsilon RI$–IgE complexes (Menon et al., 1984; Oliver et al., 1988). Analysis of our data clearly supports the existence of the two states of the $Fc_\epsilon RI$–ligand complexes at all temperatures examined (including 4 °C), thus suggesting that ligand internalization is not a factor affecting the validity of our conclusions.

Examination of the temperature dependence of the interaction between the $Fc_\epsilon RI$ and the four monovalent ligands employed in this study provides some further insights. Two different patterns may be discerned in terms of the activation characteristics of the association rate constant k_{12} (Table II). Those of Fab-F4 and Fab-J17 involve a considerable entropic barrier but have only small enthalpic contributions. In contrast, the binding rates of Fab-H10 and IgE are determined by an enthalpic barrier. The entropic contribution is negligible for Fab-H10, whereas for IgE, higher activation entropy lowers the overall activation barrier. The dissociation rates (k_{21}) of

Fab-J17 and Fab-F4 are predominantly affected by entropic barriers. The enthalpic contribution is negligible for Fab-F4 but provides about 20% of the activation barrier for Fab-J17. The ligand-induced l → h transition of the $Fc_\epsilon RI$–ligand complexes (k_{23}) encounters a large entropic barrier which is counteracted by respective negative enthalpic contributions. The reverse (h → l) transition, however, is controlled by a barrier that has both enthalpic and entropic contributions.

Comparison of the Fab-J17 and Fab-F4 barriers suggests that both the association and dissociation (step 1 of reaction R3) of these ligands encounter very similar activation barriers. The barriers to the l → h and h → l transitions (A → B and B → A), however, exhibit a similar shape yet differ in quantitative terms. The activation parameters of the association process of Fab-J17/Fab-F4 are qualitatively different from those of Fab-H10 and IgE. This finding raises the possibility that the epitopes recognized by J17/F4 are different from those of H10/IgE.

The entropic barrier of the h → l transition is practically the same for all ligands. This could suggest that the physical properties of the h conformation of the $Fc_\epsilon RI$–ligand complex do not depend on the specific ligand employed. Thus, the possibility arises that the l → h transition predominantly involves the $Fc_\epsilon RI$. It should be noted, however, that resonance energy transfer measurements suggested that a conformational transition occurs at the C2–C3 interface of IgE upon binding to the $Fc_\epsilon RI$ (Baird & Holowka, 1985; Holowka et al., 1985). This interface is proximal to the assumed combining site with the $Fc_\epsilon RI$ (Helm et al., 1985; Eshhar et al., 1990). Therefore, it may be assumed that the conformational transition involves both ligands and receptor. Further investigations are obviously necessary to resolve the nature of this structural transition.

In conclusion, this study provides evidence that the minimal reaction scheme that adequately describes the interactions between the $Fc_\epsilon RI$ on live RBL-2H3 cells and four monovalent ligands is one involving the initial formation of a $Fc_\epsilon RI$–ligand complex followed by a conformational transition of this complex from a low-affinity state l to a high-affinity state h. The equilibrium constant for this transition is of significance for Fab-H10– and IgE–$Fc_\epsilon RI$ interactions at 25 °C and for all ligands at lower temperatures. This observation clearly suggests that it is the conformational transition of the $Fc_\epsilon RI$–ligand complex which is responsible for the higher affinity and the slow dissociation rate of these ligands. While the increased affinity for IgE is per se of significance in the context of mast cell sensitization, the possibility that the conformational state of the $Fc_\epsilon RI$ may also be involved in its capacity to induce secretion upon aggregation cannot be ruled out.

An interesting finding is that rates of association and dissociation of Fab-J17 and Fab-F4 are significantly different (Table I), in spite of the fact that their receptor affinities are nearly identical (Ortega et al., 1988). Undoubtedly, the different interaction dynamics of these ligands (and the respective mAbs) with the cells might greatly influence their biological activities. This underscores the importance of complementing thermodynamic with kinetic characterization of receptor–ligand interactions as an essential basis for the understanding of ligand-induced phenomena.

ACKNOWLEDGMENTS

We are indebted to Prof. Wolfgang Dreybrodt and Dr. Ulrich Kubitscheck for critical discussions and to Prof. Leon Visser for his helpful comments on the manuscript.

APPENDIX 1. MATHEMATICAL TREATMENT OF THE SSM

To solve eq 5 describing a bimolecular reaction, we first apply the law of mass conservation, yielding

$$d[L]_b(t)/dt = k_{12}\{[Fc]_T - [L]_b(t)\}\{[L]_T - [L]_b(t)\} + k_{21}[L]_b(t) \quad (A1.1)$$

This equation can be rewritten as

$$d[L]_b(t)/dt = -k_{21}(a[L]_b(t)^2 + b[L]_b(t) + c) \quad (A1.2)$$

with

$$a = -K$$

$$b = K\{[Fc]_T - [L]_T\} + 1$$

$$c = -K[Fc]_T$$

Provided that $b^2 > 4ac$, the solution of eq A1.2 is expressed as

$$[L]_b(t) = \frac{\{[L]_{b0}(\eta^+ + 2c)\}\exp(-\tau t) - \eta^-[L]_{b0} - 2c}{2a[L]_{b0} + \eta^+ - \{2a[L]_{b0} + \eta^-\}\exp(-\tau t)} \quad (A1.3)$$

where the time constant τ is given by

$$\tau = (b^2 - 4ac)^{1/2}k_{21} \quad (A1.4)$$

and the constants $\eta^\pm$ are written as

$$\eta^\pm = b \pm (b^2 - 4ac)^{1/2}$$

$[L]_{b0}$ denotes the initial concentration of the bound ligand.

APPENDIX 2. MATHEMATICAL TREATMENT OF THE TSM

In order to solve eqs 10a–e seminumerically, we consider that each equation can be represented by the general form

$$dX_m(t)/dt = \phi(t) + c_m(t)X_m(t) \quad (A2.1)$$

where $X_1 = [L]_{b1}$, $X_2 = [L]_{b2}$, $X_3 = [Fc]_f$, $X_4 = [I]_{b1}$, and $X_5 = [I]_{b2}$. Each $X_m(t)$ corresponds to a function $\phi_m(t)$ which depends on the variables $X_1, \ldots, X_5$. The coefficient $c_m(t)$ is a function of $[L]_f$ and $[I]_f$ for $m = 3$, but it is a constant for the remaining m values. To a first approximation, we also regard ϕ_m and c_m as constants. Thus the solution of eq A2.1 is given by

$$X_m(t) = (X_{m0} + \phi_m)\exp(-c_m t) - \phi_m \quad (A2.2)$$

where X_{m0} denotes the initial concentration of the species X_m.

In the employed numerical procedure we subdivided the time period of the experiment into $m = 100$–200 time intervals δt. Equation A2.2 was then employed to calculate the concentrations $X_m(i\delta t)$ present at $t = i\delta t$ ($i = 1, 2, \ldots, m$). For the first step of the iteration process (labeled by $j = 1$) the initial concentrations X_{m0} and the values for $\phi_{m,j=1}$ and $c_{m,j=1}$ were determined by means of the concentrations X_m ($(i - 1)\delta t$) derived from the preceding step. The functions $\phi_{m,1}(i\delta t)$ are thus written as

$$\phi_{1,1}(i\delta t) = k_{12}[Fc]_f((i-1)\delta t)\,[L]_f((i-1)\delta t) + k_{23}[L]_{b2}((i-1)\delta t) \quad (A2.3)$$

$$\phi_{2,1}(i\delta t) = k_{23}[L]_{b1}((i-1)\delta t)$$

$$\phi_{3,1}(i\delta t) = k_{21}[L]_{b1}((i-1)\delta t) + k^1_{21}[I]_{b1}((i-1)\delta t)$$

$$\phi_{4,1}(i\delta t) = k^1_{12}[Fc]_f((i-1)\delta t)\,[I]_f((i-1)\delta t) + k^1_{23}[I]_{b2}((i-1)\delta t)$$

$$\phi_{5,1}(i\delta t) = k^1_{23}[I]_{b1}((i-1)\delta t)$$

The respective coefficients $c_{m,1}$ are given as

$$c_{1,1} = -(k_{21} + k_{23}) \quad \text{(A2.4)}$$

$$c_{2,1} = -k_{32}$$

$$c_{3,1}(i\delta t) = -\{k_{12}[L]_f((i-1)\delta t) + k^1{}_{12}[I]_f((i-1)\delta t)\}$$

$$c_{4,1} = -(k^1{}_{21} + k^1{}_{23})$$

$$c_{5,1} = -k^1{}_{32}$$

The concentrations $X_{m,1}(i\delta t)$ were now calculated by using

$$X_{m,1}(i\delta t) = \{X_m((i-1)\delta t) + \phi_{m,1}(i\delta t)\exp(-c_{m,1}(i\delta t)) - \phi_{m,1}(i\delta t)\} \quad \text{(A2.5)}$$

Further iteration was now carried out by calculating the functions $\phi_{m,j}(i\delta t)$ and $c_{m,j}(i\delta t)$ of the jth step. This was done by inserting the concentrations $X_{mj-1}(i\delta t)$ of the preceding iteration step instead of $X_m((i-1)\delta t)$ into eq A2.4. After convergence was obtained, the iteration was stopped and the final values for the concentrations $X_m(i\delta t)$ were calculated.

References

Austin, R. M., Beeson, K. W., Eisenstein, L., Frauenfelder, H., & Gunsalus, I. E. (1975) *Biochemistry 14*, 5355–5373.

Baird, B., & Holowka, D. (1985) *Biochemistry 24*, 6252–6259.

Berg, H. C., & Purcell, E. M. (1977) *Biophys. J. 20*, 193–219.

DeLisi, C. (1980) *Q. Rev. Biophys. 13*, 201–230.

DeLisi, C. (1981) *Mol. Immunol. 18*, 507–511.

Dembo, M., & Goldstein, B. (1978) *Immunochemistry 15*, 307–313.

Eshhar, Z. (1985) in *Hybridoma Technology in the Biosciences and Medicine* (Springer, T., Ed.) pp 3–40, Plenum, New York.

Froese, A. (1984) *Prog. Allergy 34*, 142–187.

Goldstein, B., Posner, R. G., Torney, D. C., Erickson, J., Holowka, D., & Baird, B. (1989) *Biophys. J. 56*, 955–966.

Helm, B., Marsh, P., Vecelli, D., Padlan, E., Gould, H., & Geha, R. (1988) *Nature 331*, 180–183.

Herron, J. N., Kranz, D. M., Jameson, D. M., & Voss, E. W. (1986) *Biochemistry 25*, 4602–4609.

Holowka, D., Conrad, D. H., & Baird, B. (1985) *Biochemistry 24*, 6260–6267.

Hunter, M. W., & Greenwood, F. C. (1962) *Nature 194*, 495–496.

Isersky, C., Rivera, J., Mims, S., & Triche, T. J. (1979) *J. Immunol. 122*, 1926–1936.

Ishizaka, T., Konig, W., Kurata, M., Mauser, L., & Ishizaka, K. (1975) *J. Immunol. 115*, 1078–1083.

James, F., & Ross, M. (1975) *Comput. Phys. Commun. 10*, 343–354.

Kulczycky, A., & Metzger, H. (1974) *J. Exp. Med. 140*, 1676–1695.

Menon, A. K., Holowka, D., & Baird, B. (1984) *J. Cell Biol. 98*, 577–583.

Oliver, J. M., Seagrave, J. C., Stump, R. F., Pfeiffer, J. R., & Deanin, G. G. (1988) *Prog. Allergy 42*, 185–245.

Ortega, E. (1990) Ph.D. Thesis, Feinberg Graduate School, Rehovot, Israel.

Ortega, E., Schweitzer-Stenner, R., & Pecht, I. (1988) *EMBO J. 7*, 4101–4109.

Reynolds, J. A. (1979) *Biochemistry 18*, 264–269.

Rudolph, A. K., Burrows, P. D., & Wab, M. R. (1981) *Eur. J. Immunol. 11*, 527–529.

Shoup, D., & Szabo, A. (1982) *Biophys. J. 40*, 33–39.

Smoluchowski, M. V. (1917) *Z. Phys. Chem. 92*, 129–168.

Sterk, A. R., & Ishizaka, T. (1982) *J. Immunol. 128*, 838–843.

Wank, S. A., DeLisi, C., & Metzger, H. (1983) *Biochemistry 22*, 954–959.

Zheng, Y., Shopes, A., Holowka, D., & Baird, B. (1990) *Biophys. J. 57*, 446a.